Accepted Manuscript

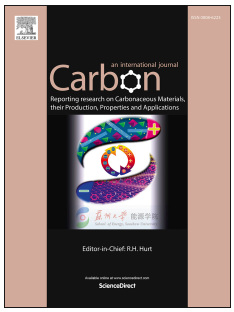

Enhanced electrical, mechanical and thermal properties by exfoliating graphene platelets of larger lateral dimensions

Tao Wang, Matthew Quinn, Shannon M. Notley

PII: S0008-6223(17)31267-8

DOI: 10.1016/j.carbon.2017.12.034

Reference: CARBON 12664

To appear in: *Carbon*

Received Date: 27 October 2017

Revised Date: 6 December 2017

Accepted Date: 9 December 2017

Please cite this article as: T. Wang, M. Quinn, S.M. Notley, Enhanced electrical, mechanical and thermal properties by exfoliating graphene platelets of larger lateral dimensions, *Carbon* (2018), doi: 10.1016/j.carbon.2017.12.034.

Enhanced Electrical, Mechanical and Thermal Properties by Exfoliating Graphene Platelets of Larger Lateral Dimensions

A way to highly effectively produce graphene sheets with large lateral dimension in aqueous solution is demonstrated by combining electrochemical and ultrasonic methods. Electrical and mechanical properties of graphene film materials fabricated with these graphene sheets are largely improved. As well, polymer-graphene composites can be prepared conveniently both for water soluble polymers and for organic soluble polymers.

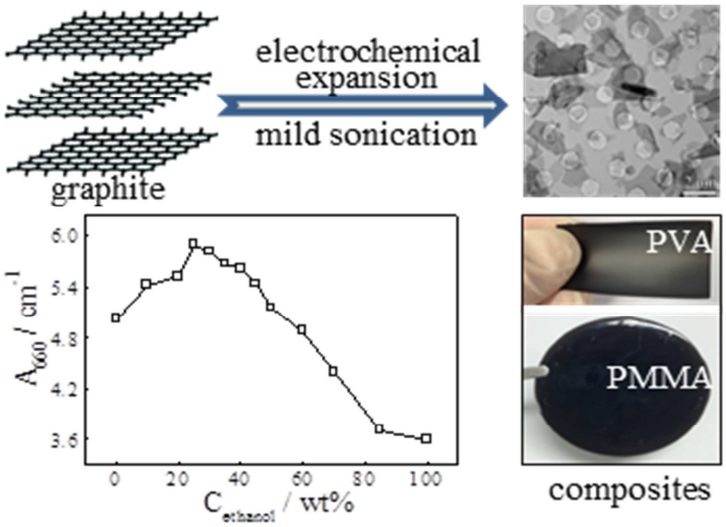

Enhanced Electrical, Mechanical and Thermal Properties by Exfoliating Graphene Platelets of Larger Lateral Dimensions

Tao Wang[1]*, Matthew Quinn[2], Shannon M. Notley[2]*

[1]*School of Materials Science and Engineering, Nanchang University, Nanchang, Jiangxi 330031, China.*
[2]*Department of Applied Mathematics, Research School of Physics and Engineering, The Australian National University, Canberra, ACT 2601, Australia.*

Abstract

Conventional liquid-phase graphite exfoliation (LPE) dramatically reduce the lateral dimension of graphene sheets to submicrometer levels due to bond cleavage induced by high shearing force or long processing time, resulting in highly degraded properties of graphene materials. Herein, a modified high-yielding LPE for producing graphene in the cosolvents of ethanol and water is demonstrated, via the prior use of an electrochemical expansion process on graphite. The electrochemically expanded graphite allows the use of significantly lower sonication power and shorter sonication times. Therefore graphene platelets with largely increased lateral dimension were achieved compared to conventional LPE (the size can reach up to 10 micrometers). The electrical and mechanical properties of graphene film are significantly enhanced as a result, with the electrical conductivity doubled and the modulus increased by a factor of 4 as well as a considerably higher areal capacitance for the assembled solid supercapacitor. Furthermore, a type of multifunctional benzoxazine surfactant was used to stabilize graphene sheets, which can also facilitate to transfer graphene sheets into organic solvents from aqueous dispersions. On this basis, polymer-graphene

* Corresponding authors. Tel: +86-79183969554. E-mail: wangt0715@ncu.edu.cn (Tao Wang); shannon.notley@anu.edu.au (Shannon M. Notley).

nano-composites have been easily prepared for both water soluble poly(vinyl alcohol) (PVA) and organic soluble poly(methyl methacrylate) (PMMA) with improved mechanical properties and thermal diffusivity.

1. Introduction

The two-dimensional (2D) material graphene has attracted attention as a promising nanomaterial for use in diverse applications such as electronic devices, energy storage devices and nano-composites [1-3]. With the sp^2 bonded carbon atoms, pristine graphene sheets have extraordinary properties including electron mobility, mechanical strength and thermal conductivity [3-6]. There are many top-down and bottom-up methods to produce graphene, all with advantages and challenges [7-12]. Methods involving chemical modifications to generate graphene oxide (GO) with subsequent reduction can produce reduced graphene oxide (rGO) with high yield and large flake size, however introduce significant basal-plane defects that will degrade the intrinsic properties of graphene [13-15] or require subsequent special reduction methods [9,16]. Scalable production routes for high quality graphene are crucial for the development of graphene applications yet still remain a challenge [10,17]. Liquid-phase graphite exfoliation (LPE) is regarded as a promising scalable route for achieving this goal by avoiding introducing basal-plane defects on graphene platelets [10,18-20]. This includes ultrasonic or shearing exfoliation in proper solvents [10,20-22].

The properties of many graphene based materials also strongly depend on the lateral dimensions of graphene sheets, as larger sheet dimensions will reduce the contact resistance between sheets caused by the boundary/edge defects [23-25]. Nevertheless, extensive LPE processing using high shearing force or long processing time can dramatically reduce the lateral dimensions. Moreover, the exfoliation yield is notably low even though graphitic sediment is recycled [10,26]. Expanded graphite has been proposed to facilitate the LPE process such as by thermal expansion [27] or ion intercalation [28]. Recently, the electrochemical method has been proposed, which includes an electrochemical expansion process and a subsequent LPE process. The prior use of electrochemical expansion on graphite facilitates the LPE process thereby leading to high production efficiency, as well as larger sheet dimensions [24,29-31]. Therein to be eco-friendly and economical, this electrochemical expansion process could be carried out in aqueous solutions [24,32]. On the contrary, the subsequent LPE process is often to be conducted in selected organic solvents in order to match the solid-liquid interfacial energy, such as 1,2-dichlorobenzene, diphenyl ether, N-methyl pyrrolidone (NMP) or dimethylformamide (DMF) [24,29]. These solvents are commonly unfavorable due to high cost, toxicity and difficult removal from the targeted materials. Water is regarded as the ideal solvent in LPE, with excellent economic and environmental benefits [21,26,31,33]. Through a rational selection of cosolvent from water and non-toxic alcohols to minimize the solid-liquid interfacial

energy difference between graphene and solvent, graphene and other 2D materials have been exfoliated successfully [20,34].

Herein we demonstrate graphene exfoliation through combining the electrochemical expansion process in aqueous electrolyte solutions and ultrasonic process in an optimized cosolvent of water and ethanol with low sonication power and short sonication time. The selection of ethanol would reduce the production cost as well as potential safety hazards. In comparison to exfoliation only involving shearing force, the usage of electrochemically expanded graphite (EEG) and a weakened sonication process lead to larger lateral dimension of graphene sheets [10,21,24,26]. This results in highly enhanced electrical conductivity and mechanical modulus.

Surfactants function to stabilize graphene sheets against reaggregation following exfoliation either by electrostatic force for ionic surfactants or by steric repulsion for nonionic surfactants [34,35]. Nevertheless surfactants with a single function are sometimes viewed as redundant or even detrimental to properties of the graphene based materials and need to be removed by extensive washing or burning out. Therefore multifunctional surfactants show potential, such as offering biocompatibility [36,37], fluorescence [38], or healing defects [39,40]. As a specific example here a curable nonionic benzoxazine surfactant (BM1000, structure and synthesis are shown in Scheme S1 and previous report [41]) was utilized. This multifunctional benzoxazine surfactant endows the graphene materials some merits such as better mechanical strength and

improved biocompatibility when assembled in a graphene film [41]. This modified exfoliation route can also avoid the surfactant degradation [41,42] as well as the evaporation of cosolvent [20] during the sonication. Moreover, the ratio of graphene to surfactant might be tuned in a wide range to fit different targeted applications due to the successful exfoliation in the optimized cosolvent in the absence of surfactants.

In some applications of graphene based materials, water is not desirable. For instance, the presence of residual water molecules will enhance charge trapping at the interface with dielectrics [43]. Likewise, graphene nanocomposites with polymers allow diverse applications in devices and sensors [32,44-46], but water has to be removed to prepare nanocomposite with water-insoluble polymers. A few works focus on transferring GO/rGO into organic solvents with some additives [47,48]. There is another desire for developing a facile way to transfer pristine graphene flakes from aqueous environment into a wide range of organic solvents, with the concentration as high as possible. Recently, we reported a versatile surfactant exchange method for atomic force microscope (AFM) characterization of 2D materials, by transferring 2D flakes into chloroform with the help of the benzoxazine surfactant of BM1000 [49]. On the basis of this method, dispersions with high graphene sheets concentration in varied organic solvents have been achieved in this work. Therefore, both water soluble and organic solvent soluble polymers could be easily fabricated through a solution process, other than that only either water soluble polymers or organic solvent polymers could be used [3,25,50]. Therein graphene flakes play an excellent role in

strengthening mechanical properties and enhancing thermal diffusivity respectively due to their large size.

2. Experimental

2.1 Production of EEG and Graphene

Graphite foil (99.8% Alfa Aesar) was used for the electrochemical reaction according to a previous report [24]. 0.1 M $(NH_4)_2SO_4$ was selected as the electrolyte, with a Pt wire as the cathode. Electrochemical expansion of graphite foil was carried out with a voltage of +10 V. Afterwards, the received EEG was filtered through a PVDF filter (0.45 μm pore size) and then extensively washed with Millipore water to remove the inorganic salt. Then the exfoliation of graphene was carried out using a Q700 Qsonica ultrasonicator with converter model CV334 and a 12.7 mm probe with replaceable tip, and a recirculating chiller was used to maintain the sonicating graphene dispersion at room temperature. Typically, the suspension of EEG in 50mL cosolvent with/without specific stabilizer was sonicated at 20% amplitude (corresponding to a power of around 20 W) for 30 min. Then the graphene dispersion obtained was centrifuged at 1500 rpm for 10 min (JOUAN centrifuge with a swing-out rotor) to remove any large unexfoliated or aggregated particles. When the concentration of EEG was used we specified the concentration of wet EEG only if demonstrated particularly.

2.2 Graphene films fabrication

Graphene films were fabricated by vacuum filtration through Anodisc membrane filters (47 mm in diameter, 20 nm pore size, Whatman). To peel graphene films easily, additional vacuum time was applied to further dry the membranes (usually overnight) after solutions were filtered out, and then reverse suction was applied by flipping the filter carrying the graphene film onto another identical filter.

2.3 Fabrication of solid state supercapacitor

The gel electrolyte was prepared firstly. 2 g PVA (average M_w 50000, ≥ 99% hydrolyzed, Aldrich) was added to 15 mL water and heated to 80 ˚C for 12 h. After cooling to room temperature, 2.0 g H_2SO_4 with 5 mL water was added dropwise. Then the mixed solution was agitated to uniform state and stored until bubbles disappeared. As prepared electrolyte was coated onto two graphene films surfaces and dried at room temperature for 12 h. Afterwards, two electrodes were pressed together gently to be assembled into an integrated device.

2.4 Characterizations

UV-visible absorption was measured on a Shimadzu spectrophotometer UV1800. FTIR was collected on a PerkinElmer Frontier FTIR spectrometer. TEM was conducted on a Hitachi H7100FA transmission electron microscope with a voltage of 75 kV. Graphene flakes were deposited on a TEM holey carbon grid using vacuum suction method. A Multimode 8 AFM from Bruker was used for imaging of the graphene flakes. Standard noncontact rectangular

cantilevers (tip radius < 10 nm, resonant frequency 300 kHz, force constant 40 N/m, Budget Sensors) were used for the tapping mode imaging. AFM samples were prepared using a Langmuir-Blodgett method by dropping chloroform dispersion onto water surface and collected using a clean silica wafer carefully. Afterwards, 350˚C calcination was used to remove surfactant and solvent. TGA was carried out on a simultaneous thermal analyzer (STA8000, PerkinElmer). The sample was heated from room temperature to 800 ºC at a heating rate of 20 ºC min^{-1} with a nitrogen flow. XPS (AXIS Nova, Kratos Analytical Ltd., Manchester, UK) was conducted using a monochromated Alkα X-ray source operating at a power of 150 W. Both survey and high resolution spectra were acquired at 160 and 20 eV pass energies, respectively. Three spots on each sample with an elliptical area approximately 300 × 700 μm^2 were analyzed. Obtained data analysis and peak fitting were performed using CasaXPS processing software version 2.3.16 (Casa Software Ltd. Teignmouth, UK). The morphology and thickness of graphene films were analyzed by a field-emission scanning electron microscope (FE-SEM, Zeiss UltraPlus). The four-point probe method (Jandel multiheight four-point probe RM3000, Jandel Engineering Ltd.) was used to measure the electrical conductivity of graphene films. Static uniaxial tensile tests were conducted with an Instron 5848 MicroTester. Graphene films were cut with a scalpel into rectangular strips of around 3 × 15 mm^2. All tests were conducted with a preload of 0.001 N and a displacement rate of 0.1 mm min^{-1}. Each type of sample was tested at least 3 times. The

sample thickness was measured from SEM images of fracture edges, and each sample was tested on at least 5 different positions to get the mean film thickness and the variability. Raman spectra were performed on a Renishaw Raman inVia Reflex with a with laser excitation at 532 nm. Graphene dispersions were deposited on membrane filter with pore size of 0.1 μm. XRD spectra were carried out on a Bruker D2 Phaser desktop diffractometer with the scanning theta range of 5º to 70º.

Cyclic voltammograms were collected on an electrochemical station (PGSTAT302N Metrohm Autolab B.V.) with a two electrode setup. All scans were run at room temperature. Areal capacitance (C_{area}) was calculated according to the equation: $C_{area} = S/(vU*s)$. S is the integration area of cyclic voltammetry data v is the scanning rate; U is the voltage range for scanning; s is the area of electrode.

Thermal diffusivity analyses were conducted on a Linseis LFA 1000 by the laser flash technique at room temperature. Pallets prepared by casting dispersion on PTFE plate were used due to the better uniformity compared with the pressed one. Each sample was shot at least 20 times to get average results. PMMA or PMMA-graphene composites were spray-coated with a thin layer of graphite according to the instrument procedure. Thermal diffusivity (α, $cm^2\ s^{-1}$) can be calculated by:

$$\alpha = 0.1388 \times I^2 / t_{1/2}$$

Where I represent thickness of test specimen in cm and $t_{1/2}$ is the time in second at 50% of temperature increase.[51]

3. Results and Discussion

Production of EEG is detailed in the Experimental section according to a previous report [24]. A thermal gravimetric analysis (TGA) (Figure S1) shows around 8.0 wt% of the EEG is expanded graphite and the rest is the residual water, which could help EEG to maintain its expanded state. Once the EEG is dried at 90 ºC, the exfoliation yield drops dramatically (Figure S2), either with or without assistance of surfactants. X-ray diffraction (XRD) confirms that the dried EEG becomes more graphitic comparing with the wet state (Figure S3). The broad peak of wet EEG indicates the disturbed stacking orientation of graphite, which facilitates to produce graphene flakes during the following weakened LPE process [6,50].

EEG was exfoliated in the cosolvents of water and ethanol at varying concentrations of ethanol (Figure 1a). In the concentration range between 20 wt% and 40 wt% corresponding to a surface tension range of 38 ~ 30 mN m^{-1} [52], higher exfoliation yields were obtained comparing to that in other ethanol concentrations. This is consistent with previous reports on the favorable liquid surface tension value for LPE [20,22]. The optimal ethanol concentration of 25 wt% for the exfoliation of EEG was obtained, which was used in the following experiments. A series of initial concentrations of EEG (C_{EEG}) were further

sonicated with and without addition of surfactants to probe the exfoliation efficiency. Interestingly, the exfoliation yield is prominent when using this low sonication power (20% amplitude, corresponding to a power of around 20 W) for a short time (10 minutes) even without the addition of surfactant. An absorption coefficient of 2460 mL mg^{-1} m^{-1} was applied to calculate graphene concentrations [21]. True initial graphite concentration (excluding the water content in wet EEG), which can be obtained via the TGA result, was divided by the graphene concentration, and then the exfoliation yield was collected in the inset in Figure 1a, which is up to 75% at the optimal ethanol concentration of 25 wt%. The graphene flakes show apparent irreversible aggregation after storage without surfactant addition. In this case, there is no significant repulsive energy barrier between graphene flakes leading to flocculation (inset, Figure S2). As shown in Figure 1b, with the addition of surfactants (benzoxazine surfactant BM1000, sodium dodecylsulfate (SDS), Pluronic surfactant F108), the exfoliation yield was improved under the same exfoliation parameters comparing with that without the addition of surfactant. This indicates that the surfactant can promote the exfoliation process, as well as stabilize the pristine graphene sheets against reaggregation. This can also be supported by the results in Figure S4 where more addition of BM1000 gave rise to higher graphene concentrations [20,34]. The exfoliation yield was further boosted to higher than 79% from a yield of 67% at the C_{EEG} of 5 mg mL^{-1} using the sonication condition of Figure 1b. With C_{EEG} of 50 mg mL^{-1} the concentration of graphene

can reach 2.7 mg mL^{-1} (Figure 1b). This concentration could be even higher with a greater initial C_{EEG} similarly to the previous work from Parvez et al [24]. Transmission electron microscopy (TEM) images of graphene flakes are shown in Figure 1c. Graphene sheets with larger lateral size and relative uniformity were obtained (most of them reach up to 2 μm), compared to those using the extensive ultrasonic method in a previous study where size of several hundred nanometers was obtained [41]. A higher resolution image in the inset of Figure 1c shows a typical layer structure (bilayer), and the selected area electron diffraction pattern shows the fine crystal lattice of the graphene flake. Typically, there is a distribution of monolayer and few-layer graphene obtained using the sonication procedure [10]. Cross sectional analysis of AFM image on several flakes in Figure 1d shows a typical thickness of ~ 0.7 nm. The sample was prepared by using a Langmuir Blodgett method according to the previous report to avoid serious aggregation [49]. This sheet thickness is consistent with the monolayer thickness from previous reports where the sonication was conducted in dimethylformamide (DMF) [30,32]. demonstrating the eminent exfoliation under the low sonication power and short sonication time. A comparison with other reported methods including conventional LPE and existing electrochemical exfoliation methods is shown in Table S1, where the advances and advantages are classified. This method presents economical and eco-friendly advantage, and receives larger graphene flakes size comparing to conventional LPE method.

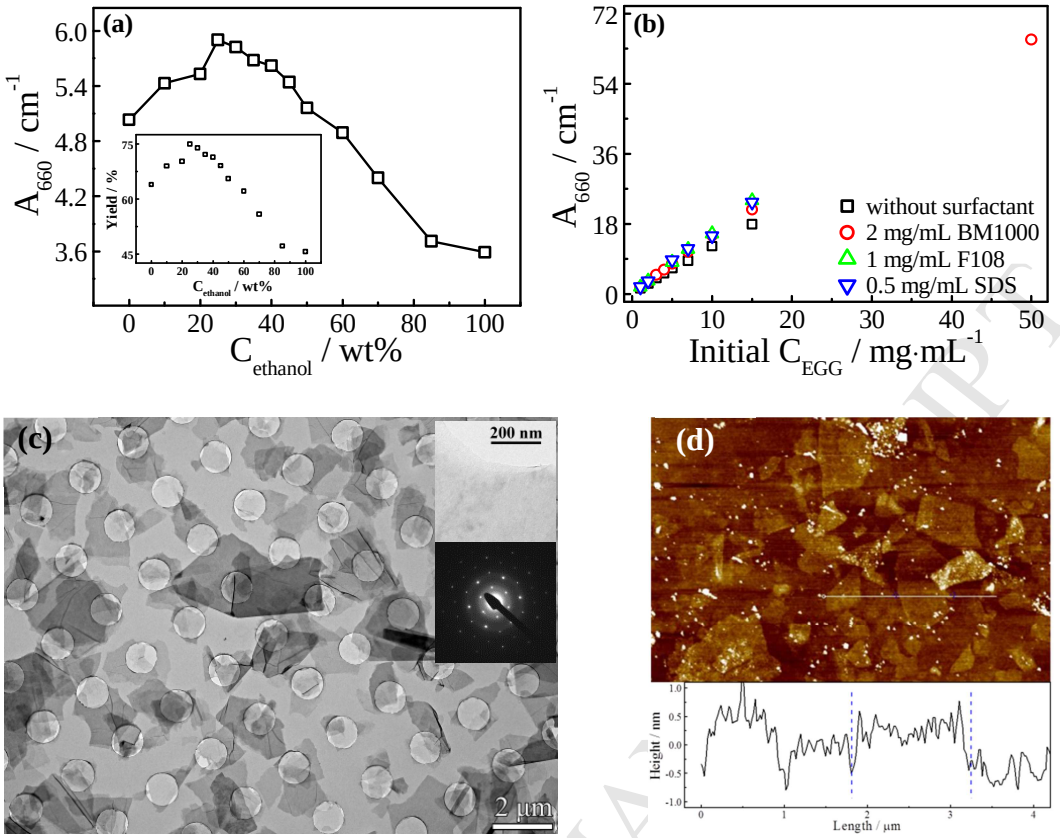

Figure 1. (a) Absorbance of exfoliated graphene suspension as a function of ethanol concentration in the cosolvent. Sonication for 10 min at 20% amplitude (a power around 20 W), C_{EEG} = 4 mg mL^{-1}, and centrifuge for 10 min at 500 rpm. Inset is the corresponding exfoliation yield at different ethanol concentration. (b) Absorbance of exfoliated graphene as a function of initial concentration of EEG (C_{EEG}) in 25 wt% ethanol with and without the addition of surfactants. All samples were sonicated for 30 min at 20% amplitude. (c) TEM imaging of graphene with the addition of BM1000. Insets are a higher resolution image and a selected area electron diffraction pattern respectively. (d) AFM image of graphene with the addition of BM1000 on a clean silica wafer and cross-sectional analysis. Sample was calcined at 350 ºC in air in a muffle furnace.

As shown in Figure 2a, electrical conductivity of up to 40 kS m^{-1} for free-standing graphene films was obtained after annealing at 250 ˚C, which is even higher than that for a rGO film thermally annealed at 500 ˚C [6]. When the benzoxazine surfactant of BM1000 was incorporated into free standing graphene films, 20 ~ 28 kS m^{-1} can be obtained after curing the surfactant (Figure 2a). This value is twice as large as before using smaller graphene sheets [41]. It is clear that the electrical conductivity only degrades slightly when BM1000 concentration increases. Sheet resistance of graphene films before and after curing is shown in Figure S6, which dropped by one order of magnitude after curing for the graphene films with BM1000 incorporated, while the graphene film without the addition of surfactant only reduced by half. This suggests that the increase in electrical conductivity for graphene films with BM1000 predominately originates from the surfactant curing, rather than the solvent removal or other factors. Better electron mobility in the matrix is achieved after curing [41]. Overlapped graphene sheets in film materials were confirmed in the scanning electron microscopy (SEM) image (Figure S5a) and the expected layered structure was observed from the cross section imaging using SEM (Figure S5b). High resolution X-ray photoelectron spectroscopy (XPS) analyses on the O1s peak deconvoluted into its components is shown in Figure 2b. The peak at 533.8 eV is attributed to the oxygen bonded on graphene boundary due to the partial oxidization on the edge during the electrochemical process. This could be caused by the radical production (e.g., HO·, which generated from water electrolysis during anodic potentials) [24,53,54]. The radicals may attack the edges of the layers to expand the graphite to

facilitate water molecules and ions intercalation. Mild degradation of graphene sheets edges happens simultaneously. In spite of these edge defects, the large lateral size of the produced graphene sheets can help abating the effects of edge defects in electrical conductivity and mechanic properties. The peak located at 532 eV originates from surfactant BM1000, with the intensity enhanced with increasing surfactant concentration used during the sonication process. Similarly, the N1s signal shows the same trend (Figure S7b), indicating that more surfactant adsorbs on the graphene sheets when higher surfactant concentration was used. Fourier-transform infrared (FT-IR) spectra confirm the incorporation of BM1000 in graphene films (Figure S8). Peaks between 1150 cm^{-1} and 1000 cm^{-1} are attributed to the polyether C-O-C stretching vibration and symmetric stretching mode of the benzoxazine ring, and peaks at 2980 cm^{-1} and 2880 cm^{-1} belong to the stretching vibration of C-H in BM1000 chain groups [41,55], which are more intensive at high BM1000 concentration both before and after curing. In addition, peaks of the polyether C-O-C stretching vibration and symmetric stretching mode of the benzoxazine ring become narrower after curing, due to the “ring opening” reaction [41].

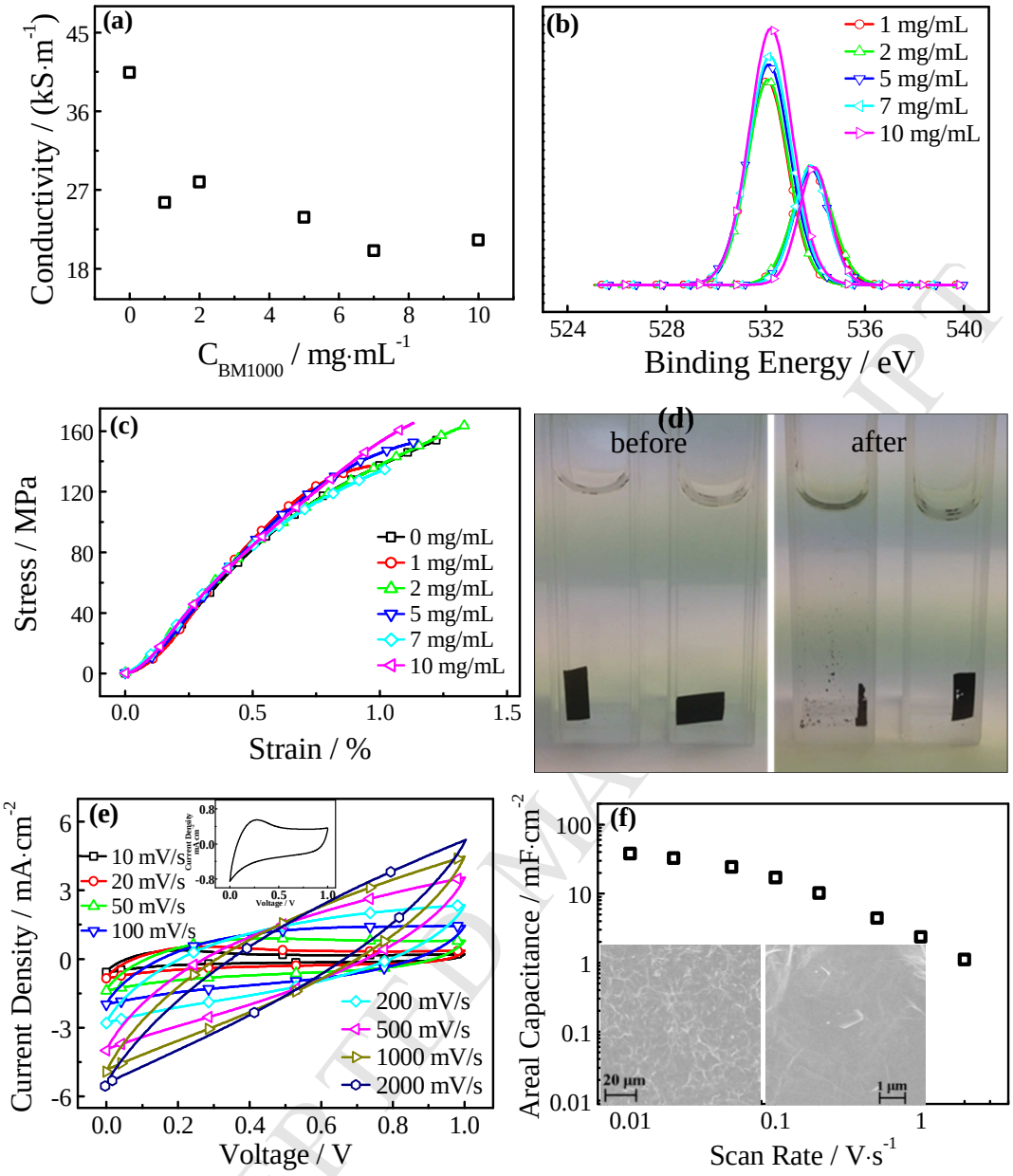

Figure 2. (a) Electrical conductivity of graphene films as the function of BM1000 concentration used in the sonication process. (b) High resolution XPS analyses on O1s of graphene films. Data has been fitted into 2 peaks using CasaXPS software. (c) Stress-strain curves of graphene films by tensile test. (d) Photographs of graphene film strips in water before sonication and after 1 min bath sonication (60 W). Strip on the left is without BM1000 and the right one is with 10 mg mL^{-1} BM1000. (e) Cyclic voltammetry curves of graphene film based supercapacitor at scan rates from 10 mV

s^{-1} to 2000 mV s^{-1}. Inset is the cyclic voltammetry data of graphene film based supercapacitor at scan rate of 20 mV. (f) Areal capacitance versus different scan rates (from 10 mV s^{-1} to 2000 mV s^{-1}) for the graphene film based supercapacitor. Insets are SEM images of a graphene film used.

A much higher modulus of ~17 GPa was obtained from tensile tests compared to the film modulus of 4.5 GPa obtained by using conventional sonication method in a previous work [41], indicating an increase in strength by a factor of 4 (Figure 2c). The better mechanical properties can be attributed to the larger graphene sheet dimensions (and aspect ratio), where connections among sheets are firmer compared to those with smaller sheets. Unlike the usual viewpoint that the surfactant residual would degrade the intriguing properties of graphene materials [21,56], tensile tests reveal that the incorporation of BM1000 did not reduce the mechanical property of graphene films, where all stress-strain curves show no significant difference in Figure 2c. Instead, the incorporation of cured BM1000 improves the graphene film performance to sustain harsh treatments such as bath sonication in liquid (Figure 2d). The film without surfactant was observed to disintegrate after undergoing 1 min of bath sonication (60 W) in water, while the structural integrity of the film with the cured BM1000 was better maintained. Samples dealed with longer sonication time (from 1 min to 10 min) are displayed in Figure S9, revealing the same trend.

The graphene films were also easily transferred onto a flexible poly(ethylene terephthalate) (PET) substrate after vacuum filtration through a hydrophobic polytetrafluoroethylene (PTFE) filter (Figure S10a). The lower surface tension of 25 wt% ethanol solution compared to water allows the liquid to freely imbibe by using ethanol to wet the PTFE filters. Conversely, graphene dispersions in water are usually filtered through inorganic hydrophilic filters, resulting in a strong interaction between graphene films and filters that makes transferring the graphene to other substrates difficult. The sheet resistance as the function of film thickness is also shown in Figure S10b, which presents similar values previously reported for graphene films containing surfactant [57]. After curing the BM1000 surfactant within the graphene film on the PET substrate, the film can resist tape adhesion and mild rubbing with an eraser (Figure S10c, d and e) [41]. Based on this method patterned conductive graphene layers on flexible substrates could be achieved [30].

The free-standing graphene film was employed to assemble a solid-state supercapacitor to demonstrate a potential application in energy storage devices. Poly(vinyl alcohol)/H_2SO_4 (PVA/H_2SO_4) gel was used as the electrolyte as well as the binding material and separator. The graphene films also served as current collectors. Different scan rates of cyclic voltammetry (CV) from 10 mV s^{-1} to 2000 mV s^{-1} were swept (Figure 2e). The nearly rectangular shape at low scan rates indicates the typical electrical double-layer capacitive behavior (inset, Figure 2e, 20 mV s^{-1}), while the oblique angle in CV curves at a high scan rate

may suggest contact resistance between graphene films and gels [58-60]. Areal capacitances at different scan rates (the calculation method is detailed in Experimental) are shown in Figure 2f. Considering the flat surface of the graphene film with a reasonable smaller active surface area compared to rough structures such as a 3D graphene network (insets, Figure 2f) [24,58,60], a considerable high areal capacitance of 38 mF cm^{-2} was achieved at a scan rate of 10 mV s^{-1}. The gravimetric capacitance can be calculated as 44 ± 1 F g^{-1} through the areal capacitance by applying the thickness of 4.3 ± 0.1 μm (from SEM characterization on cross-section) and the film density around 2.0 g cm^{-3}. This is comparable to or even higher than previous reports in regard to graphene film structures [61,62].

Polymer-graphene nanocomposites allow diverse applications. Owing to the solubility of PVA in 25 wt% ethanol solution, biomimetic nacre-like nanocomposite of graphene and PVA can be easily fabricated by mixing graphene suspension and PVA solution and drying at room temperature (Figure 3a). The typical section morphology by SEM is shown in Figure 3a with a compact lamellar microstructure within the composite. PVA molecules act as the binder to keep graphene sheets together [63], in addition to well dispersed graphene sheets in the PVA matrix. TGA shows three typical weight losses for PVA (Figure S11), corresponding to the loss of adsorbed water, elimination of water from side group and degradation of the main chain respectively. By mixing with different amounts of PVA, the proportion of graphene in the

composite can be tuned based on demand. Stress-strain curves from tensile tests on this nanocomposite with different proportions of graphene are shown in Figure 3b. A trend of higher graphene loading leads to better mechanical properties, where the large graphene sheets play the role of reinforcing agent [63,64].

In addition, the dispersibility of graphene in organic solvents is also critical for making graphene-polymer composites of water-insoluble polymers, which can reduce the agglomeration of graphene in resultant polymer matrices [3]. The amphiphilic property of BM1000 allows solubility in water and polar organic solvents. Freeze-dried graphene sample with 2 mg mL^{-1} concentration of BM1000 was well redispersed in organic solvents (such as chloroform ($CHCl_3$), dimethylformamide (DMF), dimethylacetamide (DMAc) and dimethylsulfoxide (DMSO) seeing Figure S12, but not limited to these). The dispersibility of graphene sheets with BM1000 in $CHCl_3$ allows the graphene to be directly extracted to $CHCl_3$ from aqueous dispersion (Figure 3c and Figure S13) [49]. Different concentrations of BM1000 were studied on the efficiency of extraction, and it was found that the addition of enough BM1000 (2 mg mL^{-1} BM1000 for 0.5 mg mL^{-1} graphene) can make a successful extraction of graphene sheets. TEM imaging shows that after transferred to $CHCl_3$ the graphene flakes were kept in the exfoliated state (Figure S14a). Raman spectra also support that their highly exfoliated state was well maintained after extraction to $CHCl_3$(Figure S14b). In the Raman spectra, a ratio of 0.65 of I_D/I_G suggests excellent quality of graphene sheets even though there is an obvious D peak representing the edge defects

[53]. Meanwhile, a ratio of I_D/I_{2G} smaller than 4 was obtained, which sits in the section of 3.5–4.5 for trilayer suggested by Loh et al, demonstrating a mean layer number of 3 or less [29]. This further confirms the eminent exfoliation under the low sonication power and short sonication time, and also confirms the successful transfer to $CHCl_3$.

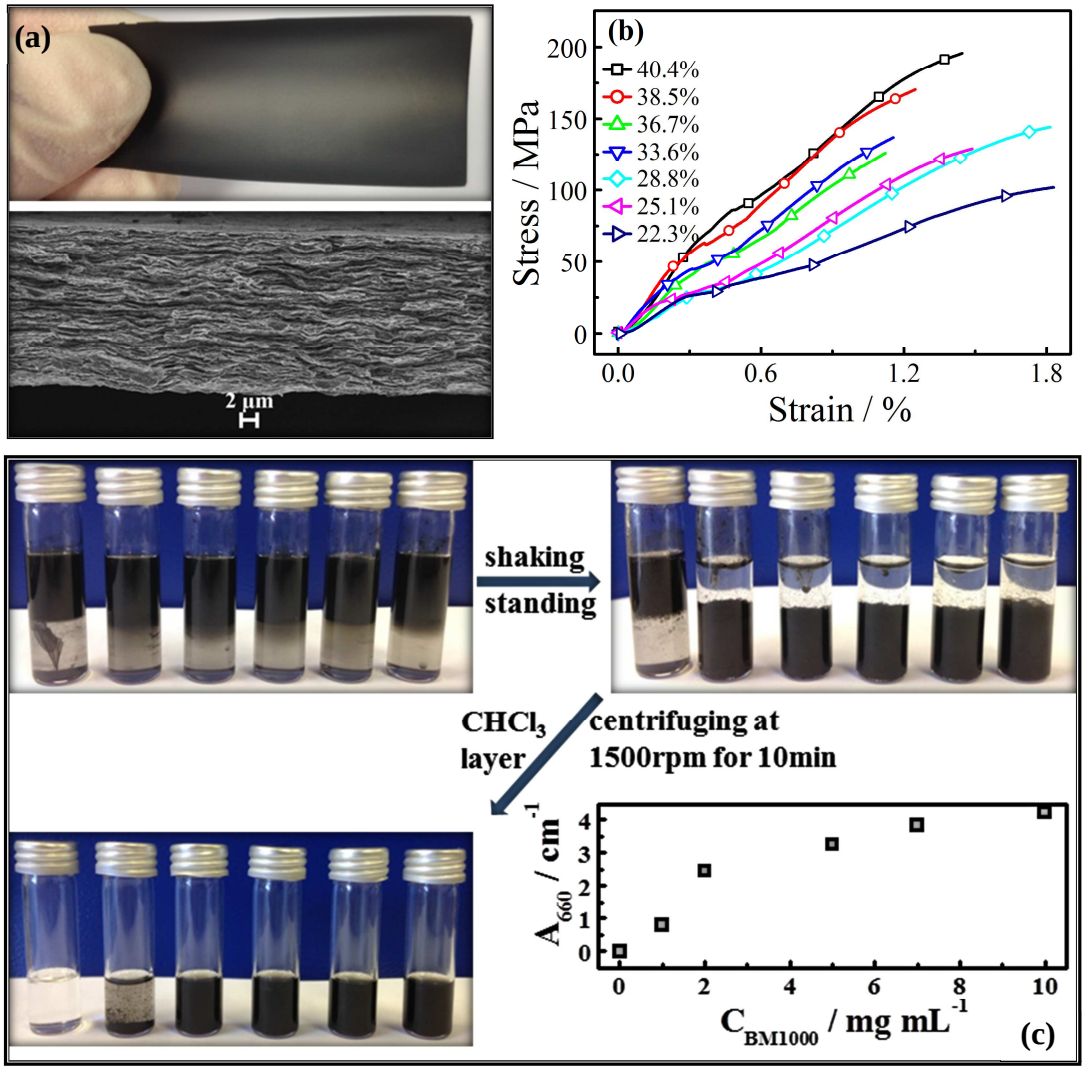

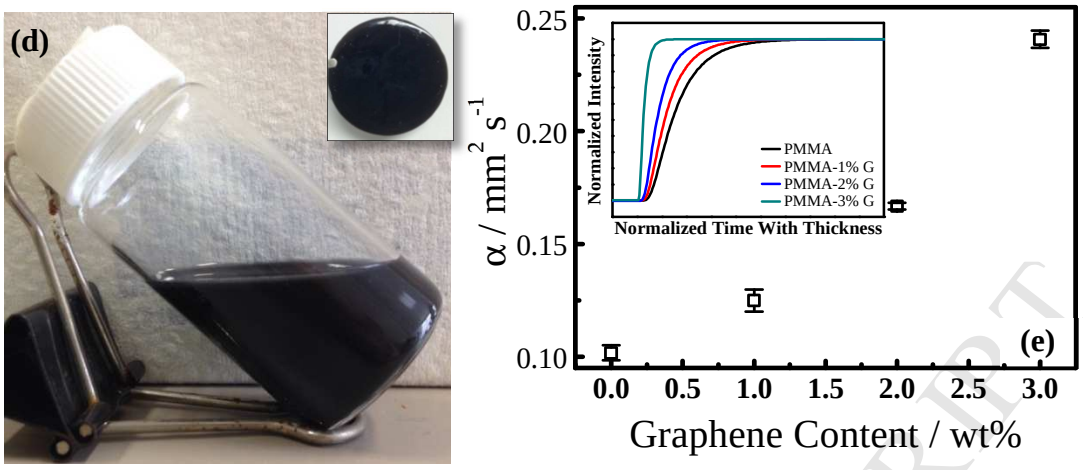

Figure 3. (a) Photograph of PVA-graphene nanocomposite film and the corresponding SEM cross section image. (b) Stress-strain by tensile test on these nanocomposite films with different graphene percentage. (c) Photographs of process transferring graphene to $CHCl_3$ from aqueous dispersion with different BM1000 concentration and the corresponding absorbance of graphene suspension in chloroform after centrifugation of 1500 rpm for 10 min. (d) Photograph of stable solution of PMMA and graphene in $CHCl_3$. Insets is the PMMA/graphene tablet by pouring dispersion onto a PTFE plate. (e) Thermal diffusivity (α) of PMMA/graphene tablet as the function of graphene content. Inset is the LFA data after normalization.

(c)

Dropping this stable graphene dispersion in chloroform onto a water surface and adopting the Langmuir Blodgett (LB) method, conductive and highly transparent graphene films could be deposited on different substrates (Figure S15). Furthermore, the extraction of larger volumes of the dispersion was carried out successfully and stable graphene dispersions in $CHCl_3$ were obtained (Figure S16). Polymer materials such as poly(methyl methacrylate)

(PMMA) are stably dissolved in the graphene suspension in chloroform (Figure 3d). Graphene loaded nanocomposites powder with PMMA was produced by precipitating in cyclohexane (Figure S17). PMMA pellets with graphene were prepared via casting the $CHCl_3$ solution onto a PTFE template or pressing nanocomposite powder via a hydraulic press (insets of Figure 3d and S17). Laser flash analysis (LFA) was performed to characterize the thermal diffusivity after incorporation of graphene into PMMA (Figure 3e). As expected, incorporation of small quantities of graphene can effectively enhance materials thermal diffusivity, due to the well dispersed graphene in the PMMA matrix and the large flake dimension to play a highly effective thermal diffusivity enhancer.

4. Conclusions

In summary, a modified LPE using low sonication power and short sonication time to produce graphene in cosolvent of ethanol and water has been developed, via the prior use of an electrochemical expansion process on graphite. This efficient method can produce graphene sheets with high yield and excellent quality. Using this method, graphene flakes with large lateral dimension were exfoliated, leading to a double electrical conductivity and an increase by a factor of 4 in modulus for graphene film materials, as well as a considerable high areal capacitance value on the assembled solid supercapacitor. In addition, the usage of cosolvent of ethanol and water allows fabricating transparent graphene films on different substrates, via vacuum filtration

through a hydrophobic PTFE filter. Furthermore, the employment of a type of multifunctional benzoxazine surfactant facilitates to transfer graphene sheets into organic solvents. Therefore polymer-graphene composites were produced both for water soluble PVA and for organic soluble PMMA, where the large graphene flakes act as excellent reinforcing agent and thermal diffusivity enhancer.

Supplementary Information

TGA of wet EEG, XRD, SEM images of graphene film, XPS of C1s and N1s of graphene films, FTIR of graphene films, photographs of transferring graphene film onto PET substrate, TGA of PVA-graphene composite, photographs of transferring graphene into chloroform, and photograph of PMMA-graphene composites.

Acknowledgements

We appreciate Desi Gharib and Dr Deming Zhu for the measurements of XPS. S.M.N. Acknowledges support from the Australian Research Council through grant FT100100177.

References

[1] El-Kady MF, Strong V, Dubin S, Kaner RB. Laser scribing of high-performance and flexible graphene-based electrochemical capacitors. Science 2012; 335(6074):1326-30.

[2] Li X, Zhang G, Bai X, Sun X, Wang X, Wang E, et al. Highly conducting

graphene sheets and Langmuir-Blodgett films. Nat Nanotechnol 2008; 3(9):538-42.

[3] Stankovich S, Dikin DA, Dommett GH, Kohlhaas KM, Zimney EJ, Stach EA, et al. Graphene-based composite materials. Nature 2006; 442(7100):282-6.

[4] Geim AK, Novoselov KS. The rise of graphene. Nat Mater 2007; 6(3):183-91.

[5] Li D, Kaner RB. Materials science - Graphene-based materials. Science 2008; 320(5880):1170-71.

[6] Chen H, Muller MB, Gilmore KJ, Wallace GG, Li D. Mechanically strong, electrically conductive, and biocompatible graphene paper. Adv Mater 2008; 20(18):3557-61.

[7] Zhu Y, Murali S, Cai W, Li X, Suk JW, Potts JR, et al. Graphene and Graphene Oxide: Synthesis, Properties, and Applications. Adv Mater 2010; 22(35):3906-24.

[8] Geim AK, Grigorieva IV. Van der Waals heterostructures. Nature 2013; 499(7459):419-25.

[9] Voiry D, Yang J, Kupferberg J, Fullon R, Lee C, Jeong HY, et al. High-quality graphene via microwave reduction of solution-exfoliated graphene oxide. Science 2016; 353(6306):1413-16.

[10] Paton KR, Varrla E, Backes C, Smith RJ, Khan U, O'Neill A, et al. Scalable production of large quantities of defect-free few-layer graphene by shear exfoliation in liquids. Nat Mater 2014; 13(6):624-30.

[11] Ciesielski A, Samori P. Supramolecular Approaches to Graphene: From Self-Assembly to Molecule-Assisted Liquid-Phase Exfoliation. Adv Mater 2016; 28(29):6030-51.

[12] Chandrashekar BN, Deng B, Smitha AS, Chen Y, Tan C, Zhang H, et al. Roll-to-Roll Green Transfer of CVD Graphene onto Plastic for a Transparent and Flexible Triboelectric Nanogenerator. Adv Mater 2015; 27(35):5210-6.

[13] Eda G, Fanchini G, Chhowalla M. Large-area ultrathin films of reduced graphene oxide as a transparent and flexible electronic material. Nature nanotechnology 2008; 3(5):270-4.

[14] Li D, Muller MB, Gilje S, Kaner RB, Wallace GG. Processable aqueous dispersions of graphene nanosheets. Nat Nanotechnol 2008; 3(2):101-5.

[15] Xiong Z, Liao C, Han W, Wang X. Mechanically Tough Large-Area Hierarchical Porous Graphene Films for High-Performance Flexible Supercapacitor Applications. Adv Mater 2015; 274469-75.

[16] Vallés C, David Núñez J, Benito AM, Maser WK. Flexible conductive graphene paper obtained by direct and gentle annealing of graphene oxide paper. Carbon 2012; 50(3):835-44.

[17] Ferrari AC, Bonaccorso F, Fal'ko V, Novoselov KS, Roche S, Boggild P, et al. Science and technology roadmap for graphene, related two-dimensional crystals, and hybrid systems. Nanoscale 2015; 7(11):4598-810.

[18] Notley SM. Highly concentrated aqueous suspensions of graphene through ultrasonic exfoliation with continuous surfactant addition. Langmuir 2012; 28(40):14110-3.

[19] Coleman JN, Lotya M, O'Neill A, Bergin SD, King PJ, Khan U, et al. Two-dimensional nanosheets produced by liquid exfoliation of layered materials.

Science 2011; 331(6017):568-71.

[20] Halim U, Zheng CR, Chen Y, Lin Z, Jiang S, Cheng R, et al. A rational design of cosolvent exfoliation of layered materials by directly probing liquid-solid interaction. Nat Commun 2013; 42213-19.

[21] Lotya M, Hernandez Y, King PJ, Smith RJ, Nicolosi V, Karlsson LS, et al. Liquid phase production of graphene by exfoliation of graphite in surfactant/water solutions. J Am Chem Soc 2009; 131(10):3611-20.

[22] Hernandez Y, Nicolosi V, Lotya M, Blighe FM, Sun Z, De S, et al. High-yield production of graphene by liquid-phase exfoliation of graphite. Nature Nanotechnology 2008; 3(9):563-8.

[23] Xiang C, Young CC, Wang X, Yan Z, Hwang CC, Cerioti G, et al. Large flake graphene oxide fibers with unconventional 100% knot efficiency and highly aligned small flake graphene oxide fibers. Adv Mater 2013; 25(33):4592-7.

[24] Parvez K, Wu ZS, Li R, Liu X, Graf R, Feng X, et al. Exfoliation of graphite into graphene in aqueous solutions of inorganic salts. J Am Chem Soc 2014; 136(16):6083-91.

[25] Lian M, Fan J, Shi Z, Zhang S, Li H, Yin J. Gelatin-assisted fabrication of graphene-based nacre with high strength, toughness, and electrical conductivity. Carbon 2015; 89279-89.

[26] Lotya M, King PJ, Khan U, De S, Coleman JN. High-concentration, surfactant-stabilized graphene dispersions. ACS Nano 2010; 4(6):3155-62.

[27] Cai M, Thorpe D, Adamson DH, Schniepp HC. Methods of graphite exfoliation.

J Mater Chem 2012; 22(48):24992.

[28] Bepete G, Anglaret E, Ortolani L, Morandi V, Huang K, Penicaud A, et al. Surfactant-free single-layer graphene in water. Nat Chem 2017; 9(4):347-52.

[29] Wang J, Manga KK, Bao Q, Loh KP. High-yield synthesis of few-layer graphene flakes through electrochemical expansion of graphite in propylene carbonate electrolyte. J Am Chem Soc 2011; 133(23):8888-91.

[30] Parvez K, Li R, Puniredd SR, Hernandez Y, Hinkel F, Wang S, et al. Electrochemically exfoliated graphene as solution-processable, highly conductive electrodes for organic electronics. ACS Nano 2013; 7(4):3598-606.

[31] Munuera JM, Paredes JI, Villar-Rodil S, Ayán-Varela M, Martínez-Alonso A, Tascón JMD. Electrolytic exfoliation of graphite in water with multifunctional electrolytes: en route towards high quality, oxide-free graphene flakes. Nanoscale 2016; 8(5):2982-98.

[32] Wei W, Wang G, Yang S, Feng X, Mullen K. Efficient coupling of nanoparticles to electrochemically exfoliated graphene. J Am Chem Soc 2015; 137(16):5576-81.

[33] Munuera JM, Paredes JI, Villar-Rodil S, Ayán-Varela M, Pagán A, Aznar-Cervantes SD, et al. High quality, low oxygen content and biocompatible graphene nanosheets obtained by anodic exfoliation of different graphite types. Carbon 2015; 94729-39.

[34] Shen J, He Y, Wu J, Gao C, Keyshar K, Zhang X, et al. Liquid Phase Exfoliation of Two-Dimensional Materials by Directly Probing and Matching Surface Tension Components. Nano Lett 2015; 15(8):5449-54.

[35] Smith RJ, Lotya M, Coleman JN. The importance of repulsive potential barriers for the dispersion of graphene using surfactants. NEW J PHYS 2010; 12(12):125008.

[36] Guan G, Zhang S, Liu S, Cai Y, Low M, Teng CP, et al. Protein Induces Layer-by-Layer Exfoliation of Transition Metal Dichalcogenides. J Am Chem Soc 2015; 137(19):6152-5.

[37] Park S, Mohanty N, Suk JW, Nagaraja A, An J, Piner RD, et al. Biocompatible, robust free-standing paper composed of a TWEEN/graphene composite. Adv Mater 2010; 22(15):1736-40.

[38] Sampath S, Basuray AN, Hartlieb KJ, Aytun T, Stupp SI, Stoddart JF. Direct Exfoliation of Graphite to Graphene in Aqueous Media with Diazaperopyrenium Dications. Adv Mater 2013; 25(19):2740-45.

[39] Geng JX, Jung H. Porphyrin Functionalized Graphene Sheets in Aqueous Suspensions: From the Preparation of Graphene Sheets to Highly Conductive Graphene Films. J Phys Chem C 2010; 114(18):8227-34.

[40] Zhang M, Parajuli RR, Mastrogiovanni D, Dai B, Lo P, Cheung W, et al. Production of graphene sheets by direct dispersion with aromatic healing agents. Small 2010; 6(10):1100-7.

[41] Wang T, Quinn MDJ, Nguyen SHT, Yu A, Notley SM. Graphene Films Using a Thermally Curable Surfactant. Adv Mater Interfaces 2016; 3(15):1600182.

[42] Wang RH, Hughes T, Beck S, Vakil S, Li S, Pantano P, et al. Generation of toxic degradation products by sonication of Pluronic (R) dispersants: implications for nanotoxicity testing. Nanotoxicology 2013; 7(7):1272-81.

[43] Ciesielski A, Samori P. Graphene via sonication assisted liquid-phase exfoliation. Chem Soc Rev 2014; 43(1):381-98.

[44] Liu Z, Parvez K, Li R, Dong R, Feng X, Mullen K. Transparent Conductive Electrodes from Graphene/PEDOT:PSS Hybrid Inks for Ultrathin Organic Photodetectors. Adv Mater 2015; 27(4):669-75.

[45] Vucaj N, Quinn MDJ, Baechler C, Notley SM, Cottis P, Hojati-Talemi P, et al. Vapor Phase Synthesis of Conducting Polymer Nanocomposites Incorporating 2D Nanoparticles. Chem Mater 2014; 26(14):4207-13.

[46] Vuluga D, Thomassin JM, Molenberg I, Huynen I, Gilbert B, Jerome C, et al. Straightforward synthesis of conductive graphene/polymer nanocomposites from graphite oxide. Chem Commun 2011; 47(9):2544-6.

[47] Liang Y, Wu D, Feng X, Müllen K. Dispersion of Graphene Sheets in Organic Solvent Supported by Ionic Interactions. Adv Mater 2009; 21(17):1679-83.

[48] Zhang C, Tjiu WW, Fan W, Huang S, Liu T. A novel approach for transferring water-dispersible graphene nanosheets into organic media. J Mater Chem 2012; 22(23):11748.

[49] Wang T, Quinn MDJ, Notley SM. A benzoxazine surfactant exchange for atomic force microscopy characterization of two dimensional materials exfoliated in aqueous surfactant solutions. Rsc Advances 2017; 7(6):3222-28.

[50] Zhang M, Huang L, Chen J, Li C, Shi G. Ultratough, ultrastrong, and highly conductive graphene films with arbitrary sizes. Adv Mater 2014; 26(45):7588-92.

[51] Parker WJ, Jenkins RJ, Butler CP, Abbott GL. Flash Method of Determining

Thermal Diffusivity, Heat Capacity, and Thermal Conductivity. J Appl Phys 1961; 32(9):1679-84.

[52] Vazquez G, Alvarez E, Navaza JM. Surface Tension of Alcohol Plus Water from 20 to 50 Degrees. J Chem Eng Data 1995; 40(3):611-14.

[53] Ambrosi A, Pumera M. Electrochemically Exfoliated Graphene and Graphene Oxide for Energy Storage and Electrochemistry Applications. Chemistry - A European Journal 2016; 22(1):153-59.

[54] Yang S, Bruller S, Wu ZS, Liu Z, Parvez K, Dong R, et al. Organic Radical-Assisted Electrochemical Exfoliation for the Scalable Production of High-Quality Graphene. J Am Chem Soc 2015; 137(43):13927-32.

[55] Sawaryn C, Landfester K, Taden A. Benzoxazine Miniemulsions Stabilized with Polymerizable Nonionic Benzoxazine Surfactants. Macromolecules 2010; 43(21):8933-41.

[56] Brownson DAC, Banks CE. Graphene electrochemistry: Surfactants inherent to graphene inhibit metal analysis. Electrochem Commun 2011; 13(2):111-13.

[57] Kang MS, Kim KT, Lee JU, Jo WH. Direct exfoliation of graphite using a non-ionic polymer surfactant for fabrication of transparent and conductive graphene films. Journal of Materials Chemistry C 2013; 1(9):1870-75.

[58] Xu Y, Lin Z, Huang X, Liu Y, Huang Y, Duan X. Flexible solid-state supercapacitors based on three-dimensional graphene hydrogel films. ACS Nano 2013; 7(5):4042-9.

[59] Conway BE, Self-Discharge of Electrochemical Capacitors in Relation to that at

Batteries, Electrochemical Supercapacitors: Scientific Fundamentals and Technological Applications, Springer US, Boston, MA, 1999, pp. 557-96.

[60] Weng Z, Su Y, Wang DW, Li F, Du JH, Cheng HM. Graphene-Cellulose Paper Flexible Supercapacitors. Advanced Energy Materials 2011; 1(5):917-22.

[61] Yoo JJ, Balakrishnan K, Huang J, Meunier V, Sumpter BG, Srivastava A, et al. Ultrathin planar graphene supercapacitors. Nano Lett 2011; 11(4):1423-7.

[62] Choi BG, Hong J, Hong WH, Hammond PT, Park H. Facilitated ion transport in all-solid-state flexible supercapacitors. ACS Nano 2011; 5(9):7205-13.

[63] Li YQ, Yu T, Yang TY, Zheng LX, Liao K. Bio-inspired nacre-like composite films based on graphene with superior mechanical, electrical, and biocompatible properties. Adv Mater 2012; 24(25):3426-31.

[64] Kuilla T, Bhadra S, Yao D, Kim NH, Bose S, Lee JH. Recent advances in graphene based polymer composites. Prog Polym Sci 2010; 35(11):1350-75.